

# Hybrid Quantum-Classical Generative Adversarial Networks with Transfer Learning

Asma Al-Othni<sup>✉</sup>, Saif Al-Kuwari<sup>✉</sup>, Mohammad Mahdi Nasiri Fatmehsari<sup>✉</sup>, Kamila Zaman<sup>✉</sup>,  
Ebrahim Ardeshtir Larijani<sup>✉</sup>



**Abstract**—Generative Adversarial Networks (GANs) have demonstrated immense potential in synthesizing diverse and high-fidelity images. However, critical questions remain unanswered regarding how quantum principles might best enhance their representational and computational capacity. In this paper, we investigate hybrid quantum-classical GAN architectures supplemented by transfer learning to systematically examine whether incorporating Variational Quantum Circuits (VQCs) into the generator, the discriminator, or both improves performance over a fully classical baseline. Our findings indicate that fully hybrid models, which incorporate VQCs in both the generator and the discriminator, consistently produce images of higher visual quality and achieve more favorable quantitative metrics compared to their fully classical counterparts. In particular, VQCs in the generator accelerate early feature learning, whereas those in the discriminator, despite exhibiting slower initial convergence, ultimately facilitate more refined synthetic outputs. Moreover, the model sustains near-comparable performance even when the dataset size is drastically reduced, suggesting that transfer learning and quantum enhancements mitigate the problem of data scarcity. Overall, the results underscore that carefully integrating quantum computing with classical adversarial training and pretrained feature extraction can considerably enrich GAN-based image synthesis. These insights open avenues for future work on higher-resolution tasks, alternative quantum circuit designs, and experimentation with emerging quantum hardware.

## 1 INTRODUCTION

IN recent years, Artificial Intelligence (AI) has advanced significantly in tasks such as image classification, language translation, and strategic gameplay. Among the different architectures pursued to tackle these tasks is generative models, which have proven especially impactful, enabling the creation of new synthetic data that can mimic or exceed real-world patterns. This capability has far-reaching implications for data augmentation and content creation,

positioning generative models as a pivotal aspect of modern AI research [1], [2], [3].

Generative Adversarial Networks (GANs) have rapidly evolved to become one of the most powerful frameworks for generative modeling, enabling the synthesis of realistic images and other high-dimensional data. Despite their remarkable achievements, GANs often struggle with issues such as training instability, mode collapse, and the need for large datasets to achieve state-of-the-art results [4]. Addressing these challenges has spurred research into new architectures and training strategies, from sophisticated loss functions to transfer learning approaches that leverage pretrained models [5], [6], [7].

Concurrently, quantum computing has made notable strides, leading to the emergence of Quantum Machine Learning (QML). QML seeks to harness quantum phenomena, such as superposition and entanglement, to enrich or accelerate classical machine learning workflows. By mapping data onto quantum states and leveraging quantum computing techniques such as parameterized quantum gates, researchers aim to achieve higher expressive power or improved optimization dynamics compared to purely classical methods [8]. One key approach involves the use of Variational Quantum Circuits (VQCs), where trainable quantum gates can transform data in ways that may surpass classical transformations, potentially enhancing tasks from classification to generative modeling. Nevertheless, the current Noisy Intermediate-Scale Quantum (NISQ) era imposes limitations such as device noise and limited qubit counts, motivating hybrid quantum-classical techniques that attempt to achieve quantum advantages, taking into account the practical hardware constraints [9], [10].

In this paper, we investigate the integration of VQCs into the GAN framework, adopting a hybrid quantum-classical approach while incorporating transfer learning. By systematically comparing fully classical and hybrid GANs, where VQCs are placed in the generator, the discriminator, or both, we explore how these quantum blocks can influence convergence behavior, image fidelity, and overall robustness. We conduct experiments on various configurations, and including multiple classes along with extended experiments featuring different sample sizes. We use quantitative metrics, including the Fréchet Inception Distance (FID), Kernel Inception Distance (KID), and Inception Score (IS), and visual inspections to provide a comprehensive assessment

Asma Al-Othni is with the Qatar Center for Quantum Computing, College of Science and Engineering, Hamad Bin Khalifa University, Doha, Qatar. E-mail: asal68497@hbku.edu.qa

Saif Al-Kuwari is with the Qatar Center for Quantum Computing, College of Science and Engineering, Hamad Bin Khalifa University, Doha, Qatar. E-mail: smalkuwari@hbku.edu.qa

Mohammad Mahdi Nasiri Fatmehsari is with the Pasargad Institute for Advanced Innovative Solutions (PIAIS), Tehran, Iran. E-mail: mehdi.nafa1373@gmail.com

Kamila Zaman is the Founder and Lead Researcher at SYLERK, Islamabad, Pakistan. E-mail: kamila.zaman@sylerk.com

Ebrahim Ardeshtir Larijani is with the Department of Mathematics and Computer Science, Iran University of Science and Technology, Tehran, Iran. E-mail: larijani@iust.ac.ir

of each model’s performance.

A key component of our approach is transfer learning, where a pre-trained ResNet-18 backbone is adapted for the discriminator to improve feature extraction. This strategy helps stabilize adversarial training, particularly under limited dataset conditions, while also allowing us to assess how quantum blocks interact with high-quality, pre-trained features. The results indicate that fully hybrid model tends to outperform other configurations, exhibiting improved convergence and producing higher-quality images. Furthermore, we show that even when the available dataset is halved, the fully hybrid architecture can still achieve outcomes close to those attained with larger datasets, highlighting the resilience and adaptability of our design.

The contributions of this research can be summarized as follows:

- Establish a solid foundation for hybrid quantum-classical GANs integrated with transfer learning
- Systematically evaluate their effectiveness against fully classical GANs and demonstrate potential quantum advantage
- Investigate how these hybrid quantum-classical methods scale when data is scarce or distributed among multiple classes

Beyond these investigations, we provide insights that lay the groundwork for future studies on high-resolution generative tasks and more advanced quantum hardware, suggesting that quantum-enhanced techniques could become a key pillar in next-generation generative modeling.

The rest of this paper is organized as follows. Section 2 provides background discussions related to GANs, QGANs and Transfer Learning. Section 3 details the proposed architecture, including generator, discriminator, variational quantum circuit, and the transfer-learning setup. Section 4 explains the experimental configurations, datasets, training setup, and evaluation metrics. Section 5 reports quantitative and qualitative results for the four binary-class experiments, and Section 6 extends the analysis to a multi-class setting. Section 7 examines learning-curve behaviour under reduced sample sizes. Finally, Section 8 concludes the paper and outlines future research directions.

## 2 PRELIMINARIES AND RELATED WORK

### 2.1 Generative Adversarial Networks

Introduced by Goodfellow *et al.* [11], Generative Adversarial Networks (GANs) are a family of deep learning models consisting of two competing neural networks, a generator and a discriminator, trained together in an adversarial process. The generator network learns to produce synthetic data (e.g., images) that closely mimic the real data distribution, while the discriminator network learns to distinguish between real samples and the generator’s synthetic samples. The GAN training procedure is formulated as a minimax (zero-sum) game: the generator strives to minimize its loss (by fooling the discriminator), whereas the discriminator strives to maximize its ability to classify real and fake data correctly. Through this adversarial training, the generator becomes increasingly skilled at creating realistic outputs, while the discriminator becomes more adept at spotting fake

inputs until the generated data is almost indistinguishable from real data. Figure 1 shows how the generator and discriminator interact within the GAN architecture.

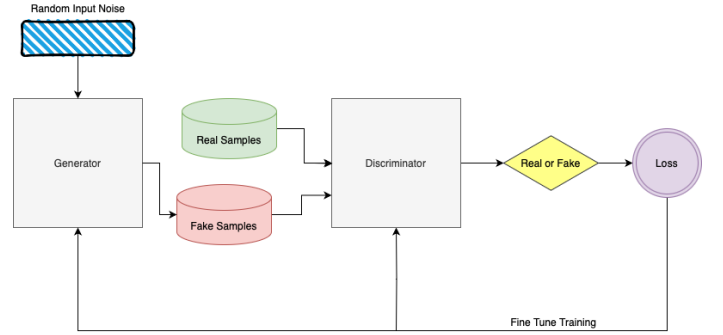


Fig. 1: Basic GAN Architecture

GAN formulates the following minimax objective for the two players (generator  $G$  and discriminator  $D$ ):

$$\min_G \max_D V(D, G) = \mathbb{E}_{x \sim p_{\text{data}}} [\log D(x)] + \mathbb{E}_{z \sim p_z} [\log(1 - D(G(z)))]$$

where  $D(x)$  is the discriminator’s estimate of the probability that the sample  $x$  is real. The generator tries to minimize this value function  $V$  (i.e., reducing  $\log(1 - D(G(z)))$  and making  $D(G(z))$  approach 1), while the discriminator tries to maximize it [11].

In practice, the generator is typically fed a source of random noise (a latent vector) and learns to transform it into realistic data samples. The discriminator is often a binary classifier that produces a probability (real or fake). They are trained in alternating steps: for a batch of data,  $D$  is updated to better distinguish real and generated samples, then  $G$  is updated to better fool  $D$ . Over many iterations, this adversarial training ideally reaches a point where the generator’s output distribution matches the real data distribution  $p_g(x) \approx p_{\text{data}}(x)$  and  $D(x) = 0.5$  for all  $x$ , indicating that the discriminator can no longer tell fake from real.

GANs are typically trained without explicit labels for the generator’s outputs; the only feedback the generator receives is from the discriminator’s judgments. This makes GANs a form of unsupervised (or self-supervised) learning [12], as the generator learns to model the data distribution without direct ground truth labels for what it generates. The discriminator provides a learning signal to the generator by grading its fakes as “real” or “not real”.

Despite the significant progress, training GANs presents several challenges. The vanishing gradient problem poses a significant challenge in GAN training. It occurs when gradients become too small during backpropagation, preventing effective weight updates. In GANs, this problem is especially pronounced due to the dynamic interaction between the generator and the discriminator. In particular, it happens when the discriminator learns too quickly, leaving the generator with minimal feedback for improvement. This issue can stall learning and contribute to mode collapse, where the generator produces a limited variation of samples, failing to capture the diversity of the real data distribution [4]. Another persistent challenge is the training instability. The adversarial dynamic between the generator and discriminator

can lead to oscillations, divergence, or mode collapse during training, necessitating careful hyperparameter tuning and monitoring. Furthermore, GANs often require large and diverse datasets for effective training [6]. The generator’s ability to produce realistic samples hinges on learning from a rich dataset, which can be a significant limitation when high-quality data is scarce.

## 2.2 Quantum Generative Adversarial Networks

Quantum Generative Adversarial Networks (QGANs) leverage quantum computing principles to improve traditional GANs [13], [14], [15]. Early QGAN implementations primarily focused on proof-of-concept models due to the constraints of near-term quantum hardware. The first QGAN models operated on minimal qubit counts, limiting them to generating low-resolution images, often as small as  $2 \times 2$  or  $4 \times 4$  pixels [16]. However, as quantum hardware improves, more sophisticated QGAN architectures have emerged. A significant milestone was achieved by Huang *et al.* [17], who demonstrated an experimental QGAN capable of generating  $8 \times 8$  grayscale handwritten digits using a superconducting quantum processor. Their approach introduced a patch-based quantum generator, where each image was divided into multiple sub-generators, each of which was processed by a dedicated quantum circuit before being reconstructed. Despite utilizing only 5 qubits per patch, QGAN successfully generated recognizable digit images. Subsequent advancements pushed the resolution of QGANs further. Tsang *et al.* [18] extended Huang’s work by generating full-resolution  $28 \times 28$  images on both MNIST and Fashion-MNIST, marking a significant step forward in quantum generative modeling.

Beyond resolution improvements, researchers have proposed various approaches to incorporate quantum computing into the GAN framework to enhance generative modeling capabilities, leading to a diverse range of QGAN architectures. For example, the QGAN model introduced in [13] employs quantum mechanical systems for the discriminator, generator, and data generation process. Similarly, the Quantum Wasserstein GAN (QWGAN) framework [19] integrates quantum circuits to compute the Wasserstein distance between real and generated distributions, a key component of the Wasserstein GAN objective [5]. Quantum Variational Autoencoders (QVAE) have also been explored in generative modeling. One such approach combines a Variational Autoencoder (VAE) with a QWGAN by integrating the VAE’s decoder into the generator of the QGAN [1]. The VAE pre-trains the generator, refining the quality of the latent space representation, which enhances training stability and sample quality. Despite this enhancement, the core training process remains adversarial, relying on the QWGAN framework. These architectural advancements demonstrate the versatility of QGANs in leveraging quantum circuits for more efficient and stable training.

More recently, alternative quantum neural architectures have been introduced to further enhance image fidelity and representation efficiency. One such development is the Quantum Implicit Neural Representation (QINR), proposed in [2], which integrates implicit neural representations (INRs) with QGANs to improve image quality while reducing the number of trainable parameters. Unlike traditional

pixel-based generative approaches, INRs represent data as continuous functions, enabling smoother, higher-resolution image synthesis. By embedding quantum circuits within the INR framework, the QINR-based QGAN exploits quantum superposition and entanglement to capture complex patterns beyond classical generative models. Empirical results indicate that QINR-based QGANs outperform traditional QGANs in sample quality while requiring fewer computational resources, making them a promising direction for further research.

While purely quantum GANs hold promise, their practical implementation remains challenging due to the current limitations of quantum hardware and the complexity of building end-to-end quantum circuits. Hybrid models, which combine classical and quantum components, offer a more realistic and accessible approach to harnessing the advantages of quantum computing. A common hybrid approach is to use a classical neural network as the generator or discriminator while integrating a quantum circuit within the other component. Tsang *et al.* [18] exemplify this hybrid strategy with a fully quantum generator that slices each  $28 \times 28$  image into 28 column patches, processes every patch through an independent five-qubit variational circuit, combines the outputs together, and forwards the composite image to a classical WGAN-GP critic. Despite using roughly three orders of magnitude fewer trainable generator parameters than a size-matched classical WGAN, their model achieves comparable visual quality on both MNIST and Fashion-MNIST. Likewise, the authors in [3] propose a hybrid GAN architecture in which the generator consists of a quantum variational circuit combined with a one-layer neural network, while the discriminator is a traditional neural network. The authors examined the performance of this quantum-classical GAN numerically by benchmarking it against a classical GAN on the task of handwritten image generation. Their results suggest that the integration of quantum circuits into the GAN framework can potentially improve the training process and the quality of the generated samples.

The progress in QGAN research reflects the broader effort to harness quantum computing for machine learning. While practical, large-scale quantum generative models are still an open challenge, recent developments in QGANs demonstrate tangible improvements in sample quality, convergence stability, and computational efficiency. As quantum hardware continues to advance, QGANs will likely play a pivotal role in next-generation generative modeling, offering unique advantages over purely classical architectures.

## 2.3 Transfer Learning

Transfer Learning (TL) is a machine learning technique in which a model trained on one task is adapted for another related task, effectively enabling the reuse of knowledge between models. This approach is particularly beneficial when labeled data for the target task is scarce, as it eliminates the need for training models from scratch, which is both computationally expensive and time-consuming. Pre-trained models, often trained on large-scale datasets, such as ImageNet [20], learn hierarchical feature representations

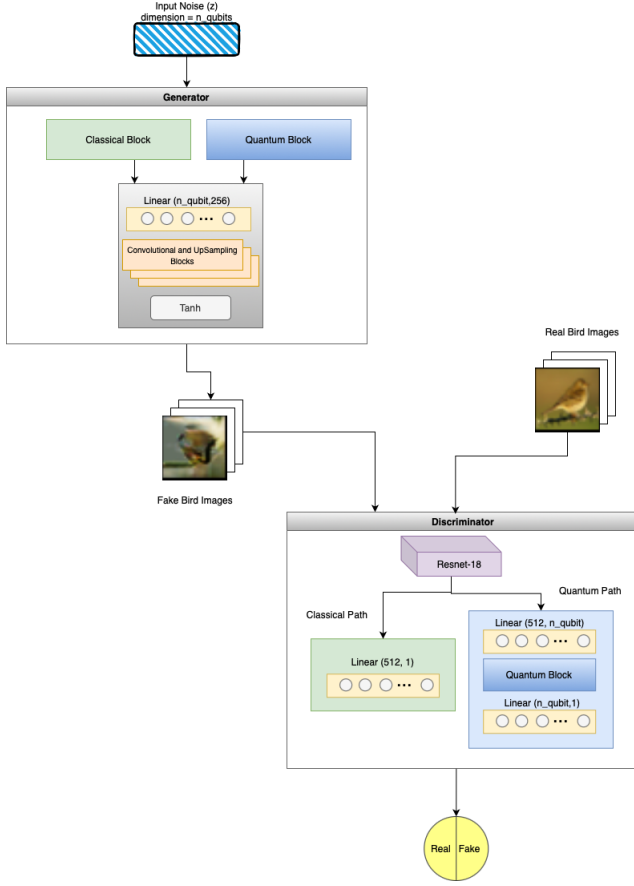


Fig. 2: Proposed Model Architecture

that can generalize well to various domains [21]. These learned features can then be either directly used as a fixed feature extractor or fine-tuned to adapt to the specific target task.

Recent research has demonstrated the effectiveness of transfer learning in image classification, showing that models pre-trained on ImageNet tend to generalize well to other classification problems [22]. This suggests that feature representations learned from large-scale datasets, like ImageNet, capture essential characteristics of images, making them valuable in a wide range of computer vision tasks [22], [23]. In [24], the authors note the common practice of transferring from ImageNet to medical imaging, indicating empirical success despite the inherent differences between natural and medical images. As a result, transfer learning has become a key technique in deep learning, significantly improving efficiency and performance in data-limited scenarios.

### 3 MODEL

In this section, we present our proposed QGAN model by describing the generator, the discriminator, the VQC we adopt in both, and the transfer-learning setup. Figure 2 illustrates the proposed model architecture corresponding to the four core configurations, which are evaluated in Section 4.

#### 3.1 Generator

As illustrated in Figure 2, the generator has two variants, one with a classical block and one with a quantum block. Apart from this first block, the rest of the architecture of the generator component is identical, ensuring that any observed performance differences arise primarily from the presence or absence of quantum blocks, rather than from broader architectural changes. The generator is structured as follows:

##### 3.1.1 Latent Vector ( $z$ )

Each training iteration begins with the sampling of a noise vector, where  $\dim(z) = n_{\text{qubits}} = 5$ . We select five qubits to keep the quantum circuit simulation computationally feasible while still affording sufficient expressiveness in the latent space. This design decision is consistent with the approach taken by [18], who constrain the latent space to low dimensions (less than 10) due to resource limitations inherent in quantum simulations, yet demonstrate that even a low-dimensional latent space can yield smooth and meaningful mappings between latent vectors and generated images.

##### 3.1.2 Learning Block

In our architecture, the learning block can either be classical or quantum. The Classical Block and the Quantum Block serve the same purpose (to process the  $n_{\text{qubits}}$ -dimensional latent vector  $z$ ), yet they do so using different mechanisms. Both blocks are designed to have a comparable number of *trainable parameters* to ensure a fair baseline for assessing quantum versus classical performance.

**3.1.2.1 Classical:** This sub-network transforms  $z \in \mathbb{R}^{n_{\text{qubits}}}$  through two fully connected layers with a ReLU in between. Concretely, it starts with a linear layer projects  $z$  from  $\mathbb{R}^{n_{\text{qubits}}}$  to  $\mathbb{R}^1$  (with no bias). Next, we have a ReLU activation to introduce nonlinearity. Finally, we add a second linear layer (with bias) that maps  $\mathbb{R}^1$  back to  $\mathbb{R}^{n_{\text{qubits}}}$ . Let  $n_{\theta}^{(\text{classical})}$  denote the total number of trainable parameters in the classical block. The first linear layer has  $n_{\text{qubits}} \times 1$  (weights only, no bias) parameters, while the second linear layer has

$$1 \times n_{\text{qubits}} (\text{weights}) + n_{\text{qubits}} (\text{biases}) = 2 n_{\text{qubits}}.$$

Hence,

$$n_{\theta}^{(\text{classical})} = (n_{\text{qubits}}) + (2 n_{\text{qubits}}) = 3 n_{\text{qubits}}.$$

For  $n_{\text{qubits}} = 5$ , this block thus contains 15 trainable parameters.

**3.1.2.2 Quantum:** In the quantum variant, a VQC is used to encode  $z$  into qubit rotations rather than purely classical linear transformations. Specifically, each component of  $z$  is loaded into the circuit via an RY rotation on a corresponding qubit. Subsequently, A chain of CNOT gates introduces entanglement among the qubits. Each qubit then undergoes a set of trainable single-qubit rotations:  $RX(\theta_{i,0})$ ,  $RY(\theta_{i,1})$ , and  $RZ(\theta_{i,2})$ . Because each qubit has three trainable parameters  $\{\theta_{i,0}, \theta_{i,1}, \theta_{i,2}\}$ , the total parameter count for the quantum block is:

$$n_{\theta}^{(\text{quantum})} = 3 n_{\text{qubits}}.$$

Thus, for  $n_{\text{qubits}} = 5$ , the circuit also contains 15 trainable parameters, which match the parameter budget of the classical block. After applying these rotations and entanglement gates, we measure the expectation value of the Pauli-Z operator on each qubit. This yields an  $n_{\text{qubits}}$ -dimensional output vector, which replaces the final output of the classical block. By constructing both blocks to produce the same dimensional output ( $\mathbb{R}^{n_{\text{qubits}}}$ ) and assigning them comparable parameter counts ( $3 n_{\text{qubits}}$ ), we ensure a balanced comparison between the quantum and classical approaches for this critical first stage of the generator. The quantum circuit architecture is discussed in detail in Section 3.3.

### 3.1.3 Fully-Connected and Batch Normalization

After the latent vector  $\mathbf{z}$  has been processed by the classical or quantum block, the resulting  $\mathbb{R}^{n_{\text{qubits}}}$ -dimensional output is mapped via a fully connected (FC) layer into a larger feature space of  $(256 \times 4 \times 4)$ . This FC layer expands the intermediate representation from a relatively small dimension (e.g., 5) to  $256 \times 4 \times 4 = 4096$  features. A one-dimensional batch normalization layer then normalizes and scales these activations across the batch, leading to more stable training and improved convergence. The resulting vector of 4096 elements is subsequently reshaped into a  $4 \times 4$  spatial grid with 256 channels, forming the initial low-resolution feature map upon which further upsampling and convolutional operations are applied.

### 3.1.4 Residual Upsampling Blocks

Two sequential Residual Upsampling Blocks gradually increase the spatial resolution of the feature maps. The first block expands the feature maps from  $(256, 4, 4)$  to  $(128, 8, 8)$ , and the second block further expands them from  $(128, 8, 8)$  to  $(64, 16, 16)$ . These blocks are designed to progressively increase spatial resolution while preserving crucial information via shortcut (residual) connections. In each block, as illustrated in Figure 3, the input feature map is first upsampled using nearest-neighbor interpolation, which doubles its height and width. The upsampled output is then refined through a series of standard convolutional layers (each followed by batch normalization and a ReLU activation). Concurrently, a  $1 \times 1$  convolution is applied to the upsampled input to align the channel dimensions with the output of the convolutional path. This alignment enables an element-wise addition between the two paths, ensuring that the original features are preserved and that the gradient flow remains smooth, thereby mitigating the vanishing or exploding gradients commonly encountered in deeper networks.

This approach is inspired by recent advances in GANs, where a step-by-step increase in resolution, combined with residual connections, has been shown to stabilize training yielding higher-fidelity synthetic images [25]. By incrementally building up to the final resolution (e.g.,  $32 \times 32$ ), these modules provide the generator with a robust mechanism to integrate both coarse and fine features, ultimately improving image realism and reducing common training instabilities.

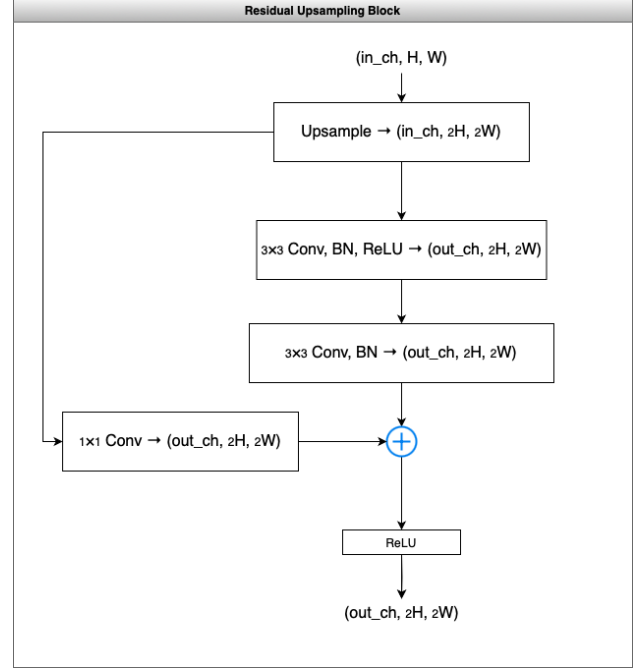


Fig. 3: Residual Upsampling Block

### 3.1.5 Final Upsampling and Convolution

After the second residual upsampling block, the feature map is further upsampled using nearest-neighbor interpolation, increasing its spatial dimensions from  $(64, 16, 16)$  to  $(64, 32, 32)$ . Subsequently, a final  $3 \times 3$  convolution is applied to project the 64 channels down to 3 output channels corresponding to the RGB color channels. This final convolution refines the upsampled features, producing the synthesized image with the desired resolution and color format.

### 3.1.6 Tanh Output

A hyperbolic tangent ( $\tanh$ ) activation function is applied to the final output of the generator, scaling the pixel intensities to the range  $[-1, +1]$ . This normalization is consistent with the preprocessing of CIFAR-10 images, which are also normalized to  $[-1, +1]$ .

## 3.2 Discriminator

The discriminator likewise has two variants, a fully classical variant and a hybrid variant that appends a quantum block to the final layers. Both start from the ImageNet-pretrained ResNet-18 weights described in Section 3.4. All input images (originally  $32 \times 32$ ) are resized to  $224 \times 224$  to be compatible with the ResNet-18 backbone.

### 3.2.1 Fully Classical Discriminator

In the fully classical setting, we leverage the pretrained ResNet-18 backbone for robust feature extraction. To tailor ResNet-18 for our GAN framework and the low-resolution CIFAR-10 images, we make several key modifications:

- 1) The original  $7 \times 7$ , stride-2 *conv1* is replaced with a  $3 \times 3$ , stride-1 convolution wrapped in *spectral\_norm* to preserve spatial detail in  $32 \times 32$  images and to stabilise GAN training.

- 2) The standard ResNet-18 architecture includes a max-pooling layer early in the network to quickly reduce spatial dimensions. However, since our inputs are low-resolution images (e.g.,  $32 \times 32$  images), preserving fine-grained spatial details is critical to differentiate between real and generated images. Removing the max-pooling layer ensures that these details are maintained throughout the network.
- 3) The final fully connected (FC) layer of ResNet-18, originally used for classification, is replaced with an identity function, which outputs a 512-dimensional feature vector. This modification retains the rich feature representation for further processing, rather than constraining it to a fixed classification space.

After these modifications, a linear layer maps the 512-dimensional feature vector to a single scalar value for real/fake discrimination.

### 3.2.2 Hybrid Discriminator

In the case of a hybrid discriminator, we retain the ResNet-18 backbone with the same adaptations (*conv1* re-sizing, *max-pool* removal, and identity mapping of the final FC layer) to extract a 512-dimensional feature vector. The subsequent layers are modified as follows:

- 1) **Projection to  $n_{\text{qubits}}$ :** A linear layer projects the 512-dimensional feature vector to a lower-dimensional space of size  $n_{\text{qubits}}$ . This projection aligns the feature vector with the input required by the quantum block.
- 2) **Quantum Block:** The  $n_{\text{qubits}}$ -dimensional vector is processed by a variational quantum circuit (similar to the one used in the generator). This circuit applies trainable single-qubit rotations and entangling gates, returning a vector of the same dimension.
- 3) **Final Linear Output:** A final linear layer maps the output of the quantum block to a single scalar value for real/fake discrimination.

By integrating a quantum block into the final classification layers in the hybrid configuration of the discriminator, we aim to leverage potential advantages from richer, non-classical decision boundaries.

### 3.3 Variational Quantum Circuit

This integration of quantum circuits into classical neural architectures reflects a broader trend in hybrid quantum-classical learning systems, where quantum layers are “dressed” with classical pre-processing or post-processing components. Such configurations, often referred to as *dressed quantum circuits*, have been shown to improve flexibility and training dynamics, especially in scenarios involving transfer learning [26].

Our model deploys these dressed quantum blocks in the generator, discriminator, or both, while maintaining a unified circuit design that balances expressive power with computational feasibility. Figure 4 shows the circuit diagram used in this project, which includes:

- 1) **Data Encoding:** Each qubit’s rotation angle (RY gate) is set to a specific component of the input vector,

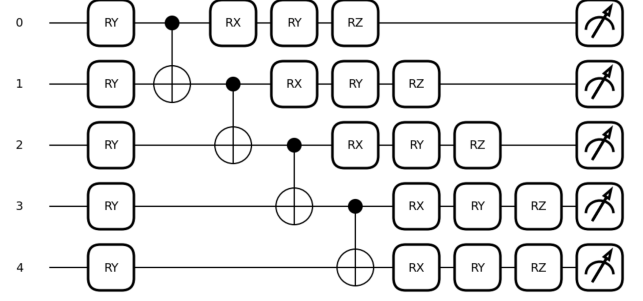


Fig. 4: Quantum Circuit Diagram

whether that vector represents latent noise (in the generator) or projected features (in the discriminator). This step embeds classical data into the quantum state.

- 2) **Entanglement:** Sequential CNOT gates between neighboring qubits introduce correlations that are difficult to replicate in purely classical networks. By tying the qubits’ states together, the circuit can learn richer representations.
- 3) **Trainable Gates:** Each qubit undergoes parameterized single-qubit rotations  $RX(\theta_{i,0})$ ,  $RY(\theta_{i,1})$ , and  $RZ(\theta_{i,2})$ . The circuit thus has  $3 \times n_{\text{qubits}}$  learnable parameters, tuned via backpropagation to improve performance. Keeping  $n_{\text{qubits}}$  relatively small ensures that simulation overhead remains manageable.
- 4) **Measurement:** Finally, the circuit measures each qubit in the Pauli-Z basis, returning a real-valued expectation value per qubit. For a batch of size  $N$ , this yields an  $(N, n_{\text{qubits}})$  output tensor of expectation values, which is then passed to the next stage of the network (e.g., a fully connected layer or the generator’s upsampling blocks).

This coherent framework for data encoding, entanglement, learnable rotations, and measurement provides a non-classical feature transformation, offering advantages over purely classical architectures.

During each training iteration, the discriminator is updated by computing a loss from real images (labeled as 1) and images generated by the generator (labeled as 0), and then backpropagating the sum of these losses to update its parameters. Subsequently, the generator is optimized to produce images that the discriminator misclassifies as real. This adversarial training loop forms the backbone of our experimental framework and provides a robust foundation for comparing fully classical and hybrid quantum-classical architectures.

### 3.4 Transfer Learning

Compared to the extensive exploration and proven success of transfer learning in discriminative tasks, such as image classification and object detection, its application to generative tasks, particularly image synthesis, has received relatively less attention [6]. Recent studies have shown that transfer learning can also be beneficial in improving

the performance of GANs in target domains with limited data [6], [7]. A key common insight from these studies is that the low-level filters of a pre-trained GAN discriminator, which capture general visual features like edges and textures, can be effectively leveraged to aid generation in the target domain. By freezing or fine-tuning the low-level layers of the discriminator, and only training the higher-level layers, the generator can be guided to produce more realistic samples, even when the target dataset is small. In contrast, the generator must typically be trained from scratch or carefully fine-tuned, as its task of learning a novel and specific data distribution rarely benefits from previously learned discriminative features. This distinction emphasizes why practitioners commonly apply transfer learning to discriminators to expedite GAN training and enhance image quality, stability, and convergence speed [27], [28].

Following the discriminator design in Section 3.2, we apply transfer learning exclusively to the discriminator network. Specifically, we load the ImageNet-pretrained ResNet-18 weights released by He *et al.* [29], apply our architectural modifications, and fine-tune all layers. The pre-training provides robust edge and texture detectors, while full fine-tuning enables the model to adapt entirely to the CIFAR-10 domain and the adversarial training objective, without the risk of freezing suboptimal filters. The architectural changes described earlier (*conv1* resizing, removal of the early *max-pool*, and replacement of the final FC layer with *Identity*) are applied to both discriminator variants prior to fine-tuning. ResNet-18 is selected for its balance between computational efficiency and representational performance, offering a lightweight yet effective backbone for transfer learning on CIFAR-10 within hybrid quantum-classical workflows.

## 4 EVALUATION

Our work comprises four primary configurations (Experiments 1–4) along with Experiment 5, which is an extension of Experiment 4. The key variations lie in the integration of quantum blocks within the generator and/or the discriminator. Specifically, Experiment 1 employs a fully classical architecture for both the generator and the discriminator; Experiment 2 uses a classical generator with a quantum-enhanced discriminator; Experiment 3 utilizes a quantum-enhanced generator while retaining a fully classical discriminator; and Experiment 4 integrates quantum blocks in both the generator and the discriminator. Experiment 5 further examines the model under more demanding conditions, including multiple classes and a longer training duration.

To evaluate performance, we employ a comprehensive set of metrics, including adversarial training losses, extended quantitative measures such as the Fréchet Inception Distance (FID), Inception Score (IS), and Kernel Inception Distance (KID), as well as qualitative assessments via visual inspection of generated images. Together, these metrics allow for a detailed analysis of convergence, training stability, and the overall quality of the generated images.

## 4.1 Experiments

The purpose of this research is to explore the integration of quantum computing elements into Generative Adversarial Networks (GANs), specifically focusing on their impact when combined with classical transfer learning techniques in the discriminator. We propose four core experimental setups, each training on a reduced CIFAR-10 dataset (initially filtering only the “Bird” class). The experiments vary by whether the generator and/or discriminator contain quantum blocks. Finally, in experiment 5, we extend the fourth experiment to investigate multiple classes (Birds, Cars, Dogs) with longer training schedules (500 epochs) and varying sample sizes to assess scalability and robustness. The five core experiments conducted in this study are as follows:

- **Experiment 1 (Baseline, Fully Classical):** A classical generator paired with a classical discriminator utilizing transfer learning. This serves as the reference model for evaluating quantum enhancements.
- **Experiment 2 (Classical Generator, Hybrid Discriminator):** A classical generator is combined with a hybrid discriminator that integrates both transfer learning and a quantum processing block.
- **Experiment 3 (Hybrid Generator, Classical Discriminator):** A quantum-enhanced generator is trained alongside a classical discriminator that incorporates transfer learning.
- **Experiment 4 (Fully Hybrid, Single-Class):** Both the generator and the discriminator employ quantum processing components, alongside transfer learning in the discriminator.
- **Experiment 5 (Fully Hybrid, Multi-Class):** To further assess the robustness and generalizability of the fully hybrid model (Experiment 4), we conducted extended experiments under more demanding conditions. In these extended experiments, the scope was broadened beyond the single “Bird” class by performing separate runs on three distinct classes: Birds, Cars, and Dogs. Moreover, the training duration was increased from 100 epochs to 500 epochs, thereby enabling a deeper analysis of long-term stability and scalability in a hybrid quantum-classical setting. For evaluation, we compared image quality and training dynamics using two different sample sizes: one experiment utilized 5,000 samples, and another employed 2,500 samples. This comprehensive evaluation framework facilitates a detailed examination of the fully hybrid architecture’s performance under diverse data regimes and extended training durations.

## 4.2 Dataset

All experiments utilize the CIFAR-10 dataset, which contains 60,000 color images of size 32×32 spanning 10 classes. Because the discriminator uses a pretrained ResNet-18 (originally trained on ImageNet), we require 3-channel RGB images to match the network’s expected input format, and CIFAR-10 conveniently provides color images in that shape. Moreover, CIFAR-10’s relatively small resolution and

simpler content reduce computational overhead, which is particularly important when simulating quantum circuits, allowing for faster training iterations.

For the initial 100-epoch runs of each experiment, we filter the dataset to include only the “Bird” class (index 2), thus isolating a single object category and focusing on the generative capabilities without the multi-class confusion. In Experiment 5, we broaden this scope by including three classes, Birds (index 2), Cars (index 1), and Dogs (index 5), and increasing training to 500 epochs, thus assessing how the fully hybrid quantum-classical architectures scale with multiple classes and longer training schedules.

In our experiments, after filtering CIFAR-10 for the target (Birds) class, 5,000 images from the training set are used for model training. Since the CIFAR-10 test set contains about 10,000 images, filtering it for the target class yields roughly 1,000 images for evaluating generative performance. Using this held-out test subset for evaluation ensures that our performance metrics are computed on images not seen during training. Moreover, all images are loaded in batches of size 8 to accommodate quantum-circuit overhead, and normalized to the range  $[-1, +1]$  across each channel.

### 4.3 Training Setup

The training setup for our GAN experiments is designed to balance computational efficiency with training stability, particularly given the overhead associated with quantum circuit simulations. All experiments use a consistent batch size of 8, which ensures that even the hybrid quantum-classical models are trained within the available hardware/simulation constraints. For Experiments 1 through 4, each model is trained for 100 epochs to evaluate the convergence and performance differences, while Experiment 5 (incorporating multiple classes of Birds, Cars, and Dogs) is trained for 500 epochs to assess scalability and long-term stability. We utilize the Adam optimizer with a learning rate of  $2 \times 10^{-4}$  and momentum parameters  $\beta = (0.5, 0.999)$ , settings that are standard in the GAN literature and effective for preventing mode collapse by smoothing gradient updates. The Binary Cross-Entropy with Logits loss function (BCEWithLogitsLoss) is applied to both the generator and discriminator, allowing the discriminator’s output to be interpreted as raw logits while avoiding numerical issues associated with separate sigmoid activations.

### 4.4 Evaluation Metrics

We assess the performance of our GAN models using a multifaceted evaluation framework. First, we monitor the generator and discriminator losses, which provide initial insights into the adversarial training dynamics. Second, we perform periodic visual inspections by generating sample images to subjectively assess realism and diversity. Third, we compute extended quantitative metrics to rigorously evaluate the quality of the generated images. These metrics include the Fréchet Inception Distance (FID), the Kernel Inception Distance (KID), and the Inception Score (IS).

Fréchet Inception Distance (FID): FID measures the distance between the feature distributions of real and generated images. It is computed as:

$$\text{FID} = \|\mu_r - \mu_g\|^2 + \text{Tr}\left(\Sigma_r + \Sigma_g - 2\left(\Sigma_r \Sigma_g\right)^{\frac{1}{2}}\right),$$

where  $\mu_r$  and  $\Sigma_r$  denote the mean and covariance of the features extracted from real images, and  $\mu_g$  and  $\Sigma_g$  denote those of the generated images. Lower FID values indicate that the two distributions are closer, implying that the generated images more closely resemble the real ones.

Kernel Inception Distance (KID): KID is based on the squared Maximum Mean Discrepancy (MMD) using a polynomial kernel, and it provides an alternative measure that is less sensitive to the choice of feature space while offering an unbiased estimate with finite sample sizes. KID is defined as:

$$\text{KID} = \frac{1}{n(n-1)} \sum_{i \neq j} k(x_i, x_j) + \frac{1}{m(m-1)} \sum_{i \neq j} k(y_i, y_j) - \frac{2}{nm} \sum_{i,j} k(x_i, y_j),$$

where  $x_i$  and  $y_i$  represent the features of real and generated images respectively,  $n$  and  $m$  are the number of real and generated samples, and  $k(\cdot, \cdot)$  is a polynomial kernel function (e.g.,  $k(a, b) = \left(\frac{a^\top b}{d} + 1\right)^3$ ). Lower KID scores similarly indicate a closer match between the distributions.

Inception Score (IS): IS evaluates both the quality and diversity of generated images. It is calculated as:

$$\text{IS} = \exp\left(\mathbb{E}_x \left[ D_{\text{KL}}(p(y|x) \| p(y)) \right]\right),$$

where  $p(y|x)$  is the conditional probability distribution of labels given an image  $x$  as predicted by a pretrained Inception network, and  $p(y)$  is the marginal distribution of the overall generated images. A higher Inception Score indicates that the generated images are both diverse and of high quality.

Collectively, these metrics offer a robust evaluation framework: lower FID and KID scores signal better performance, while a higher Inception Score indicates better generative quality.

## 5 BINARY CLASSIFICATION RESULTS

In this section, we evaluate the performance of the four experimental binary-class configurations, where the model is trained to generate images from a single class (birds). We report both quantitative findings (loss curves, FID, KID, and IS) and qualitative insights based on the generated images.

### 5.1 Quantitative Evaluation

Our Quantitative evaluation consists of loss and metrics analysis. In the loss analysis, we examine the generator and discriminator loss curves over 100 epochs. In the metric analysis, we compare the four experiments using FID, KID, and IS to quantify the fidelity and diversity of the images.

#### 5.1.1 Loss Results

Figures 5a through 5d present the generator (orange) and discriminator (blue) loss curves over 100 epochs for the four experimental configurations. By comparing these curves, we can observe distinct patterns of convergence and training stability in each model.

**5.1.1.1 Experiment 1: Classical Generator with Classical Discriminator:** In this baseline model, the discriminator’s loss starts at a moderate level and gradually declines before stabilizing in the lower loss range. Concurrently, the generator’s loss rises steadily for the first 30 epochs and then plateaus in the 4-5 range. This interplay suggests that the classical discriminator consistently learns to classify real and fake samples, while the classical generator, although initially challenged, manages to stabilize at a moderately high loss-implying it continues to struggle against the discriminator without collapsing.

**5.1.1.2 Experiment 2: Classical Generator with Hybrid Discriminator:** In this experiment, only the discriminator incorporates a quantum block. The discriminator’s loss drops more sharply in the early epochs but then stabilizes at very low levels, reflecting a heightened capacity to distinguish real from fake images. The generator’s loss, meanwhile, spikes significantly (peaking around epoch 30) and remains at a higher overall level compared to Experiment 1. This behavior indicates that the quantum-enhanced discriminator provides a stronger adversary, pushing the classical generator to higher and somewhat more volatile loss values.

**5.1.1.3 Experiment 3: Hybrid Generator with Classical Discriminator:** When the generator is augmented with a quantum block, but the discriminator remains classical, the discriminator’s loss stabilizes above zero but does not exhibit the sudden drops seen in Experiment 2. The generator’s loss remains elevated, though more steadily, suggesting that the quantum generator may be producing more complex or higher-quality samples. Consequently, the classical discriminator faces a consistent challenge, but its slower decline indicates that it is still adapting effectively without being overwhelmed.

**5.1.1.4 Experiment 4: Hybrid Generator with Hybrid Discriminator:** In the fully hybrid model, both networks incorporate quantum blocks. The discriminator’s loss drops rapidly in the early epochs, mirroring some patterns seen in Experiment 2, but fluctuates less dramatically. The generator’s loss initially spikes (similarly to Experiment 2) and then settles in a moderately high range, indicating sustained adversarial tension. The overall pattern suggests that both networks are leveraging quantum features, leading to a more intense, yet relatively balanced, interplay where neither side dominates conclusively.

Taken as a whole, these loss plots underscore how the introduction of quantum blocks into the discriminator typically imposes a tougher learning environment for the generator, as evidenced by higher or more volatile generator losses. Conversely, a quantum-enabled generator appears to produce samples that challenge a classical discriminator more consistently, though without the steep oscillations seen when the discriminator itself is quantum-augmented. Ultimately, the fully hybrid model (Experiment 4) combines these dynamics, offering a more competitive and sustained adversarial interaction.

### 5.1.2 Metrics Results

Table 1 summarizes the FID, KID, and IS for each experiment. Lower FID and KID values indicate that the generated images are closer to the real-image distribution, whereas a

Ex	Generator	Discriminator	FID	KID	IS
1	Classical	Classical	349.6	0.321	1.822
2	Classical	Hybrid	328.4	0.251	2.351
3	Hybrid	Classical	257.4	0.145	2.722
4	Hybrid	Hybrid	198.7	0.088	2.393

TABLE 1: Comparison of FID, KID, and IS Across Four Experiments

higher IS implies better quality and diversity in the generated samples.

The baseline model (Experiment 1) exhibits the highest FID (349.6) and KID (0.321), along with the lowest IS (1.822). This fully classical setup struggles to match the performance of the hybrid models. By introducing a quantum block into the discriminator (Experiment 2), FID decreases to 328.4 and KID to 0.251, while IS increases to 2.351. Although this outperforms Experiment 1, it does not represent the best overall outcome. When only the generator is quantum-enhanced (Experiment 3), FID improves to 257.4, KID to 0.145, and IS to 2.722 (the highest among all experiments). This suggests a notable gain in image diversity. In the fully hybrid model (Experiment 4), both FID and KID reach their lowest values (198.7 and 0.088, respectively), indicating the closest distributional alignment with real images. IS remains relatively high at 2.393, but slightly below Experiment 3.

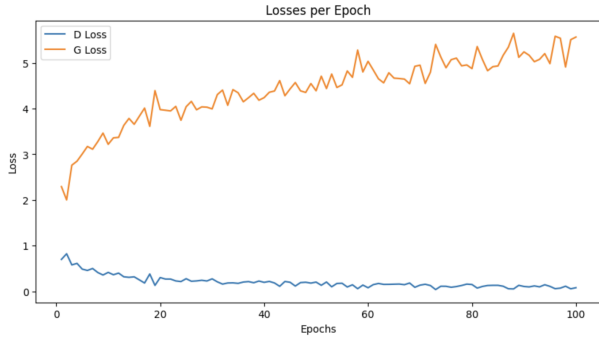
However, it is important to acknowledge the biases and limitations of certain evaluation metrics. As noted by [30], FID can be biased toward specific datasets, given its reliance on feature embeddings from a pre-trained inception network. Similarly, IS has been criticized for its unreliability in capturing the actual realism of the generated samples. Therefore, relying on additional metrics such as KID, which is less prone to domain-specific biases, is crucial for a more comprehensive evaluation of generative performance.

## 5.2 Qualitative Evaluation

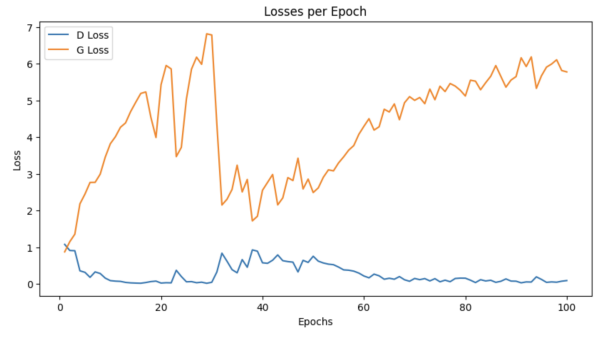
One key observation that we can conclude from visually analyzing the generated images is that when the discriminator includes a quantum block but the generator remains classical (as in Experiment 2, Figure 6b), the model appears to converge slower in the early epochs – reflected by the highly abstract and less-defined outputs at epochs 1, 5, and 30. In contrast, placing the quantum block in the generator (Experiment 3, Figure 6c) seems to accelerate the initial learning process; even within the first few epochs, the model begins to form rudimentary bird outlines, suggesting that the quantum-enabled generator rapidly captures essential structural information compared to the other models. In the fully hybrid setup (Experiment 4, Figure 6d), the generator’s quantum capacity competes with the quantum-enhanced discriminator, which again introduces some early-stage volatility but ultimately leads to more refined images. Overall, these observations reinforce that the location of the quantum block (generator vs. discriminator) significantly influences the speed and character of convergence during the initial phases of training.

## 6 MULTI-CLASS CLASSIFICATION RESULTS

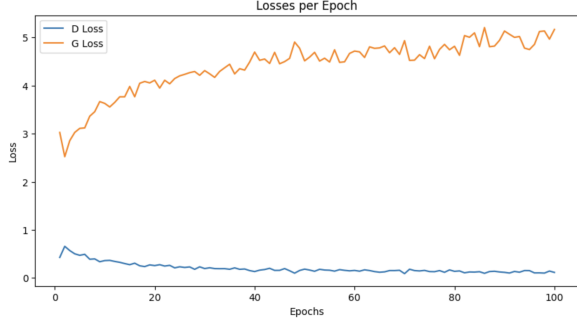
In this section, we present the results of Experiment 5, where we evaluate our model on a multi-class classification



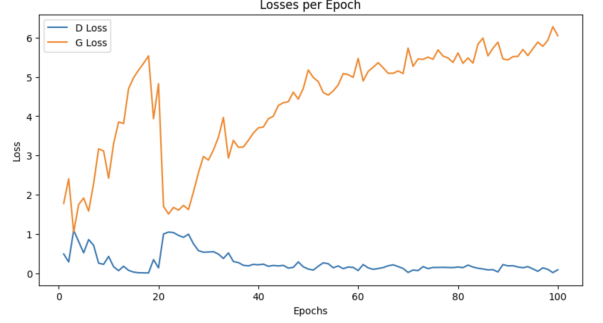
(a) Losses Plot of Experiment 1



(b) Losses Plot of Experiment 2



(c) Losses Plot of Experiment 3



(d) Losses Plot of Experiment 4

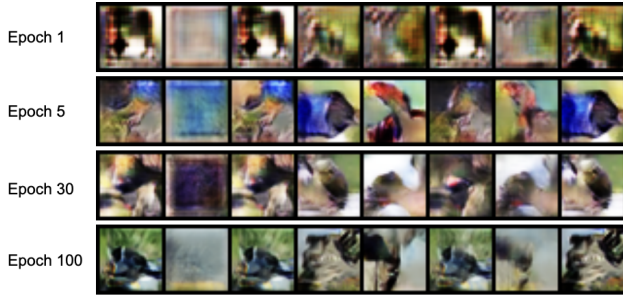
Fig. 5: Loss Plots of Experiments 1 - 4



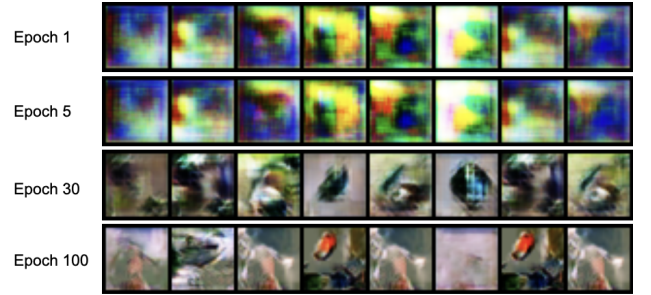
(a) Generated Samples from Experiment 1



(b) Generated Samples from Experiment 2



(c) Generated Samples from Experiment 3



(d) Generated Samples from Experiment 4

Fig. 6: Generated samples from Experiments 1 - 4

problem. Unlike the binary classification experiments we conducted in Section 5, in this section, we focused on the fully quantum variant of our model as it was the one that outperformed all other variants in the binary classification problem.

## 6.1 Quantitative Evaluation

When trained on multiple classes (Birds, Cars, Dogs) in a fully hybrid setting (Experiment 5), the model typically enters a strong learning phase during the first 100–200 epochs, showing noticeable gains in quality and diversity as evident in Figures 7a, 7b, and 7c. Beyond 200 epochs, the

rate of improvement gradually slows down, and training enters a phase of incremental refinements rather than dramatic gains. This is particularly noticeable for challenging classes like Birds, where finer details remain difficult to synthesize effectively. Although extending training to 500 epochs results in some additional refinements, the diminishing improvements indicate that the model approaches convergence. Minor oscillations observed in later epochs suggest that the adversarial dynamics between the generator and discriminator reach an equilibrium but continue to fluctuate slightly.

While the hybrid architecture can handle complex, multi-class data effectively, the key takeaway is that the majority of significant improvements emerge in the first few hundred epochs and a plateau in progress (verified by stable scores and qualitative inspection), generally indicates the model is near convergence.

## 6.2 Qualitative Evaluation

Figures 8a, 8c, and 8b illustrate the progression of generated samples at different training stages (epochs 100, 200, 300, 400, and 500). These visualizations confirm that most substantial improvements occur within the first 200 epochs, after which refinements are more gradual, supporting the earlier observation that the model reaches near-convergence around epoch 200.

## 7 LEARNING CURVE RESULTS

When the sample size is reduced to 2,500 per class, the early training stages (epoch 0-200) show increased volatility and slower convergence compared to the 5,000-sample runs. However, as training progresses, the key metrics, such as FID (Figure 9a), KID (Figure 9b), and IS (Figure 9c), eventually converge to levels that are comparable to those achieved with a larger sample size in Figures 7a, 7b, and 7c.

To further validate the observed stability in the 2500-sample setting, Figures 10a, 10b and 10c, present the qualitative evolution of generated images across training epochs. Despite an initially noisier training process, the generator progressively refines object structures and textures, producing coherent outputs comparable to those from the larger dataset. These results confirm that our hybrid quantum-classical approach, combined with transfer learning, stabilizes training even under data-limited conditions.

This suggests that despite the initial instability, the model is able to capture the essential features required for high-quality image synthesis even with fewer samples. The observed behavior is likely due to the robust learning afforded by our hybrid quantum-classical architecture and transfer learning approach. Thus, while the reduced sample size introduces some early challenges, the overall convergence remains nearly similar.

## 8 CONCLUSION

In this paper, we explore the integration of Variational Quantum Circuits (VQCs) and transfer learning techniques into Generative Adversarial Networks (GANs), focusing on hybrid architectures that incorporate quantum enhancements in the generator, the discriminator, or both. Through

a systematic experimental evaluation, we assessed the performance of various configurations across multiple datasets and training conditions, providing strong empirical evidence that hybrid quantum-classical GANs offer tangible benefits over purely classical approaches. The significance of this work lies in its demonstration of how quantum computing principles can enhance generative modeling by improving convergence efficiency, representation capacity, and sample fidelity. Furthermore, by leveraging transfer learning, we incorporated pre-trained feature extractors into the discriminator, which helped improve learning efficiency and maintain performance even in lower-data scenarios, suggesting its role in enhancing the robustness and scalability of hybrid models. By bridging quantum computing and deep learning, this research contributes to the ongoing effort to leverage near-term quantum devices for practical machine learning applications.

Our results demonstrate that incorporating quantum blocks into the GAN architecture enhances both the qualitative and quantitative performance of the generated images. The fully hybrid model, which integrates quantum blocks in both the generator and the discriminator, consistently outperforms the fully classical baseline as well as the mixed configurations. Notably, a quantum-enabled generator accelerates early convergence and better captures intricate structural details, while a quantum-enhanced discriminator provides a more challenging adversarial signal that ultimately leads to improved image fidelity. Furthermore, even with reduced sample sizes, the model converges to performance levels comparable to those achieved with larger datasets, underscoring the robustness of our approach. These findings suggest that quantum components can enhance the expressive power of GANs, thereby opening new avenues for future research focused on optimizing hybrid quantum-classical architectures and extending their applications to high-resolution image synthesis and other complex generative tasks.

## REFERENCES

- [1] A. M. Thomas and S. T. Jose, "Vae-qwgan: Improving quantum gans for high resolution image generation," *arXiv preprint*, vol. arXiv:2409.10339, 2024. [Online]. Available: <https://arxiv.org/abs/2409.10339>
- [2] Q. Ma, C. Hao, N. Si *et al.*, "Quantum adversarial generation of high-resolution images," *EPJ Quantum Technology*, vol. 12, p. 3, 2025.
- [3] R. Shu, X. Xu, M.-H. Yung, and W. Cui, "Variational quantum circuits enhanced generative adversarial network," 2024. [Online]. Available: <https://arxiv.org/abs/2402.01791>
- [4] G. Iglesias, E. Talavera, and A. Díaz-Álvarez, "A survey on gans for computer vision: Recent research, analysis and taxonomy," *Computer Science Review*, vol. 48, p. 100553, 2023.
- [5] M. Arjovsky, S. Chintala, and L. Bottou, "Wasserstein generative adversarial networks," in *Proceedings of the 34th International Conference on Machine Learning*, vol. 70, 2017, pp. 214–223. [Online]. Available: <http://proceedings.mlr.press/v70/arjovsky17a.html>
- [6] M. Zhao, Y. Cong, and L. Carin, "On leveraging pretrained gans for generation with limited data," *arXiv preprint arXiv:2002.11810*, 2020. [Online]. Available: <https://arxiv.org/abs/2002.11810>
- [7] J. Lv, G. Li, X. Tong, W. Chen, J. Huang, C. Wang, and G. Yang, "Transfer learning enhanced generative adversarial networks for multi-channel mri reconstruction," *Computers in Biology and Medicine*, vol. 134, p. 104504, 2021.
- [8] T. A. Ngo, T. Nguyen, and T. C. Thang, "A survey of recent advances in quantum generative adversarial networks," *Electronics*, vol. 12, no. 4, p. 856, 2023.

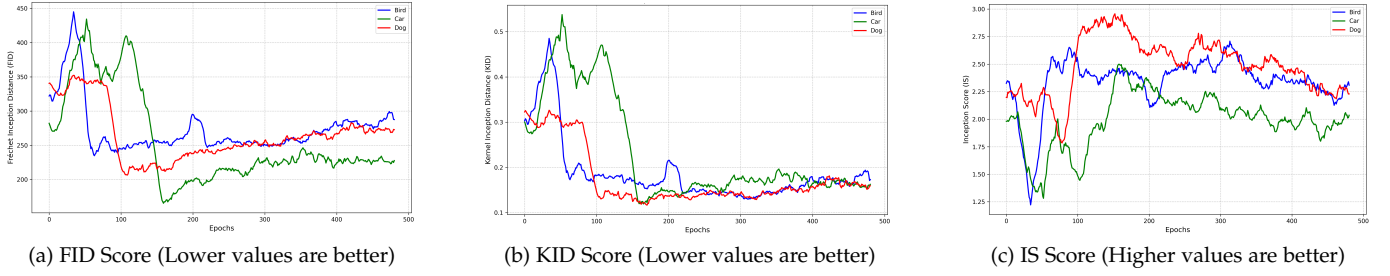


Fig. 7: FID, KID and IS scores for multiclass classification with 5000 samples

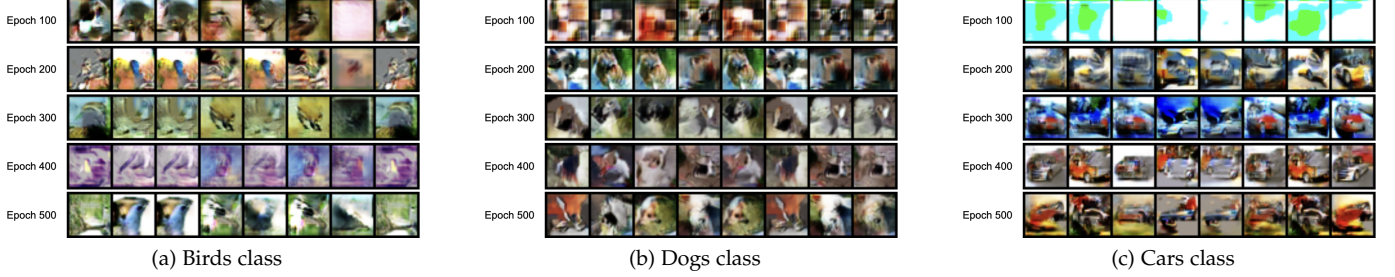


Fig. 8: Generated Samples from Experiment 5 with 5000 samples

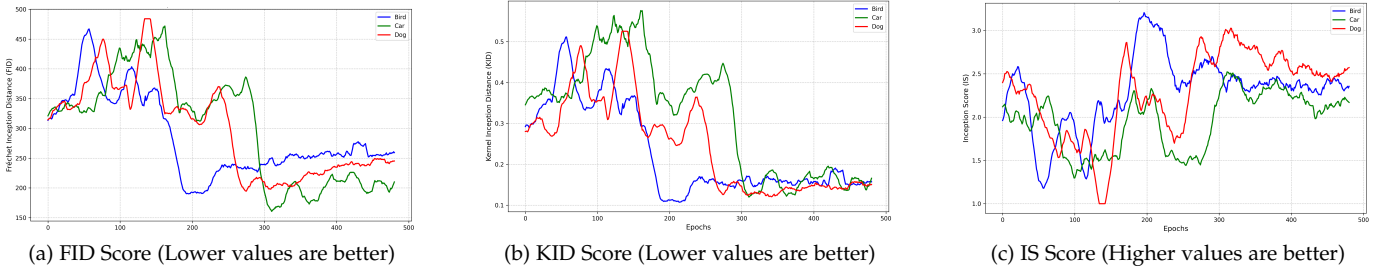


Fig. 9: FID, KID and IS scores for multiclass classification with 2500 samples

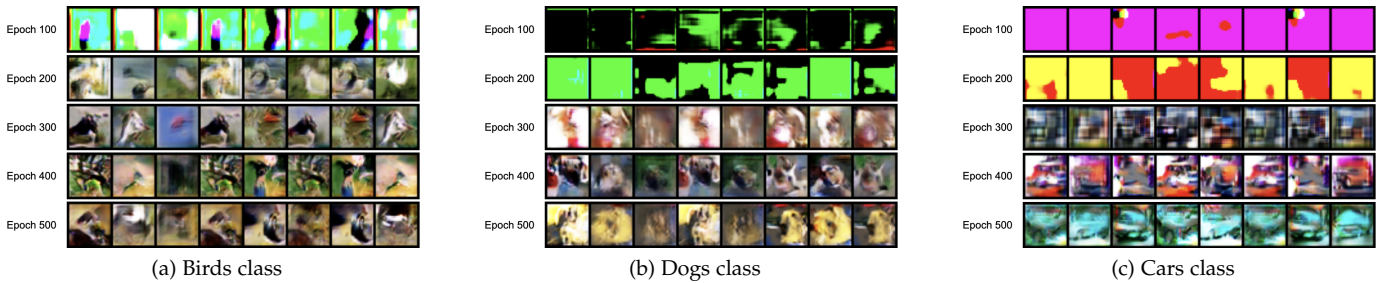


Fig. 10: Generated Samples from Experiment 5 with 2500 samples

- [9] K. Bharti, A. Anand, D. Das, S. W. Lee, A. Beitia, T. Shi, M.-H. Yung, V. Vedral, and L. C. Kwek, "Noisy intermediate-scale quantum algorithms," *Reviews of Modern Physics*, vol. 94, no. 1, p. 015004, 2022.
- [10] A. Callison and N. Chancellor, "Hybrid quantum-classical algorithms in the noisy intermediate-scale quantum era and beyond," *Physical Review A*, vol. 106, no. 1, p. 010101, 2022.
- [11] I. Goodfellow, J. Pouget-Abadie, M. Mirza, B. Xu, D. Warde-Farley, S. Ozair, A. Courville, and Y. Bengio, "Generative adversarial nets," in *Advances in Neural Information Processing Systems*, vol. 27, 2014, pp. 2672–2680. [Online]. Available: [https://papers.nips.cc/paper\\_files/paper/2014/file/5ca3e9b122f61f8f06494c97b1afcf3-Paper.pdf](https://papers.nips.cc/paper_files/paper/2014/file/5ca3e9b122f61f8f06494c97b1afcf3-Paper.pdf)
- [12] F. Eckerli and J. Osterrieder, "Generative adversarial networks in finance: An overview," *arXiv preprint arXiv:2106.06364*, 2021. [Online]. Available: <https://arxiv.org/abs/2106.06364>
- [13] S. Lloyd and C. Weedbrook, "Quantum generative adversarial learning," *Physical Review Letters*, vol. 121, no. 4, p. 040502, 2018.
- [14] L. Hu, Y. Wu, W. Cai, Y. Ma, X. Liu, H. Wang, Y. Chen, C. Guo, D. Mei, H. Deng, D. Xu, H. Wang, Y. Xu, H. Lu, Y. Zhong, S. Yuan, H. Su, C.-Y. Lu, C.-Z. Peng, X. Zhu, and J.-W. Pan, "Quantum generative adversarial learning in a superconducting quantum circuit," *Science Advances*, vol. 5, no. 1, p. eaav2761, 2019.
- [15] M. Y. Niu, A. Zlokapa, M. Broughton, S. Boixo, M. Mohseni,

- V. Smelyanskyi, and H. Neven, "Entangling quantum generative adversarial networks," *Physical Review Letters*, vol. 128, no. 22, p. 220505, 2022.
- [16] M. Pajuhanfard, R. Kiani, and V. Sheng, "Survey of quantum generative adversarial networks (qgan) to generate images," *Mathematics*, vol. 12, no. 23, p. 3852, 2024.
- [17] H.-L. Huang, Y. Du, M. Gong, Y. Zhao, Y. Wu, C. Wang, S. Li, F. Liang, J. Lin, Y. Xu, and et al., "Experimental quantum generative adversarial networks for image generation," *Physical Review Applied*, vol. 16, p. 024051, 2021.
- [18] S. Tsang, M. T. West, S. M. Erfani, and M. Usman, "Hybrid quantum-classical generative adversarial network for high resolution image generation," 2022. [Online]. Available: <https://doi.org/10.48550/arXiv.2212.11614>
- [19] S. Chakrabarti, Y. Huang, T. Li, S. Feizi, and X. Wu, "Quantum wasserstein generative adversarial networks," *arXiv preprint*, vol. arXiv:1911.00111, 2019. [Online]. Available: <https://arxiv.org/abs/1911.00111>
- [20] J. Deng, W. Dong, R. Socher, L.-J. Li, K. Li, and L. Fei-Fei, "Imagenet: A large-scale hierarchical image database," in *Proc. IEEE Conf. Computer Vision and Pattern Recognition (CVPR)*, 2009, pp. 248–255.
- [21] X. Han, Z. Zhang, N. Ding, Y. Gu, X. Liu, Y. Huo, J. Qiu, Y. Yao, A. Zhang, L. Zhang, W. Han, M. Huang, Q. Jin, Y. Lan, Y. Liu, Z. Liu, Z. Lu, X. Qiu, R. Song, J.-R. Wen, J. Yuan, W. X. Zhao, and J. Zhu, "Pre-trained models: Past, present and future," *AI Open*, vol. 2, pp. 225–250, 2021.
- [22] S. Kornblith, J. Shlens, and Q. V. Le, "Do better imagenet models transfer better?" in *Proceedings of the IEEE/CVF Conference on Computer Vision and Pattern Recognition (CVPR)*, 2019, pp. 2656–2666.
- [23] A. Fang, S. Kornblith, and L. Schmidt, "Does progress on imagenet transfer to real-world datasets?" *arXiv preprint arXiv:2301.04644*, 2023. [Online]. Available: <https://arxiv.org/abs/2301.04644>
- [24] S. Azizi et al., "Big self-supervised models advance medical image classification," in *2021 IEEE/CVF International Conference on Computer Vision (ICCV)*, 2021, pp. 3458–3468.
- [25] T. Karras, T. Aila, S. Laine, and J. Lehtinen, "Progressive growing of gans for improved quality, stability, and variation," in *International Conference on Learning Representations (ICLR)*, 2018. [Online]. Available: <https://openreview.net/forum?id=Hk99zCeAb>
- [26] A. Mari, T. R. Bromley, J. Izaac, M. Schuld, and N. Killoran, "Transfer learning in hybrid classical-quantum neural networks," *Quantum*, vol. 4, p. 340, 2020.
- [27] M. J. Chong, K. K. Singh, Y. Li, J. Lu, and D. Forsyth, "P2d: Plug and play discriminator for accelerating gan frameworks," in *Proceedings of the IEEE/CVF Winter Conference on Applications of Computer Vision (WACV)*, 2024.
- [28] M. Mo et al., "Freezed: A simple baseline for fine-tuning gans," 2020. [Online]. Available: <https://arxiv.org/abs/2002.10964>
- [29] K. He, X. Zhang, S. Ren, and J. Sun, "Deep residual learning for image recognition," in *Proc. IEEE Conf. Computer Vision and Pattern Recognition (CVPR)*, 2016, pp. 770–778.
- [30] N. A. Alhamdi and M. E. Sunni, "Chest x-ray image synthesis using deep convolutional gans," in *2024 IEEE 4th International Maghreb Meeting of the Conference on Sciences and Techniques of Automatic Control and Computer Engineering (MI-STA)*, 2024, pp. 698–705.